Pop-out search instigates beta-gated feature selectivity enhancement across V4 layers

Jacob A. Westerberg[a,1], Elizabeth A. Sigworth[b], Jeffrey D. Schall[c], and Alexander Maier[a]

[a]Department of Psychology, Vanderbilt Brain Institute, Vanderbilt Vision Research Center, Vanderbilt University, Nashville, TN 37240; [b]Department of Biostatistics, Vanderbilt University, Nashville, TN 37240; and [c]Centre for Vision Research, Vision: Science to Applications Program, Department of Biology and Department of Psychology, York University, Toronto, ON M3J 1P3, Canada

Edited by Thomas D. Albright, Salk Institute for Biological Studies, La Jolla, CA, and approved October 26, 2021 (received for review February 23, 2021)

Visual search is a workhorse for investigating how attention interacts with processing of sensory information. Attentional selection has been linked to altered cortical sensory responses and feature preferences (i.e., tuning). However, attentional modulation of feature selectivity during search is largely unexplored. Here we map the spatiotemporal profile of feature selectivity during singleton search. Monkeys performed a search where a pop-out feature determined the target of attention. We recorded laminar neural responses from visual area V4. We first identified "feature columns" which showed preference for individual colors. In the unattended condition, feature columns were significantly more selective in superficial relative to middle and deep layers. Attending a stimulus increased selectivity in all layers but not equally. Feature selectivity increased most in the deep layers, leading to higher selectivity in extragranular layers as compared to the middle layer. This attention-induced enhancement was rhythmically gated in phase with the beta-band local field potential. Beta power dominated both extragranular laminar compartments, but current source density analysis pointed to an origin in superficial layers, specifically. While beta-band power was present regardless of attentional state, feature selectivity was only gated by beta in the attended condition. Neither the beta oscillation nor its gating of feature selectivity varied with microsaccade production. Importantly, beta modulation of neural activity predicted response times, suggesting a direct link between attentional gating and behavioral output. Together, these findings suggest beta-range synaptic activation in V4's superficial layers rhythmically gates attentional enhancement of feature tuning in a way that affects the speed of attentional selection.

attention | cortical microcircuit | LFP | visual cortex | visual search

Throughout cortex, sensory information is organized into maps. This phenomenon is readily observable in visual cortex where maps organize information in both the radial (e.g., within cortical columns) and tangential (e.g., across a cortical area) dimensions (1–4). Importantly, sensory information attributed to these maps is malleable. For example, selective attention is linked to profound changes in neural activity organizing sensory information in both space and time (5–34).

In visual cortex, cortical columnar microcircuits comprise many neurons that respond to the same location of visual space and similar stimulus features. For example, primary visual cortex (V1) features "orientation columns" consisting of neurons sharing response preference for the same stimulus orientation (35, 36) and "ocular dominance columns" consisting of neurons that preferentially respond to the same eye (37). Similar columnar organization for feature selectivity has been described across many other visual cortical areas, including area V2 (36, 38, 39), area V3 (40), middle temporal area (area MT) (41–43), and inferotemporal cortex (44–46). Midlevel visual cortical area V4, a well-studied area contributing to attentional modulation, follows suit with columnar organization of visual responses and feature preferences (44, 47–53). Yet, we do not know the extent to which attention impacts feature preferences along columns. While canonical microcircuit models of cortex predict laminar differences for attentional modulation [e.g., feedback-recipient extragranular layers modulating before granular layers (54–56)], how this modulation interacts with columnar feature selectivity is largely unknown.

We sought to determine the spatiotemporal profile of feature preferences within the V4 laminar microcircuit during attentional selection. To address this question, we performed neurophysiological recordings along V4 layers in monkeys performing an attention-demanding pop-out search task. We identified feature columns demonstrating homogeneous feature preference along cortical depth. When the search array item presented in the column's receptive field (RF) was unattended, the upper cortical layers were most selective. However, when attended, feature selectivity in the deep layers enhanced the most, resulting in overall strongest feature selectivity in both extragranular compartments. We further found that the enhancement of feature selectivity associated with attention was rhythmically gated in the beta range. While beta activity was measurable across both unattended and attended conditions, rhythmic gating of feature selectivity was only present with attention. Moreover, beta power modulating the neural response was predictive of response time (RT), suggesting a link between attentional gating and behavior. Synaptic currents revealed the beta rhythm originates in superficial cortical layers, which is compatible with top-down influence.

Results

Behavioral Performance. Both monkeys performed a pop-out visual search task necessitating attentional selection of, followed

Significance

Cerebral cortex is organized in topographical maps of cortical columns. These columns consist of mesoscopic neural circuits that preferentially respond to certain stimulus features like color. We show that attending a visual stimulus results in rhythmic gating of feature preferences along cortical columns. The strength of that rhythm directly impacts the behavioral outcome. These findings demonstrate that the dynamics of feature preferences in cortical columns underlie at least some of the rhythmicity that is associated with attention.

Author contributions: J.A.W., J.D.S., and A.M. designed research; J.A.W. performed research; J.A.W. and E.A.S. analyzed data; and J.A.W., E.A.S., J.D.S., and A.M. wrote the paper.

The authors declare no competing interest.

This article is a PNAS Direct Submission.

[1]To whom correspondence may be addressed. Email: jacob.a.westerberg@vanderbilt.edu.

This article contains supporting information online at https://www.pnas.org/lookup/suppl/doi:10.1073/pnas.2103702118/-/DCSupplemental.

Published December 10, 2021.

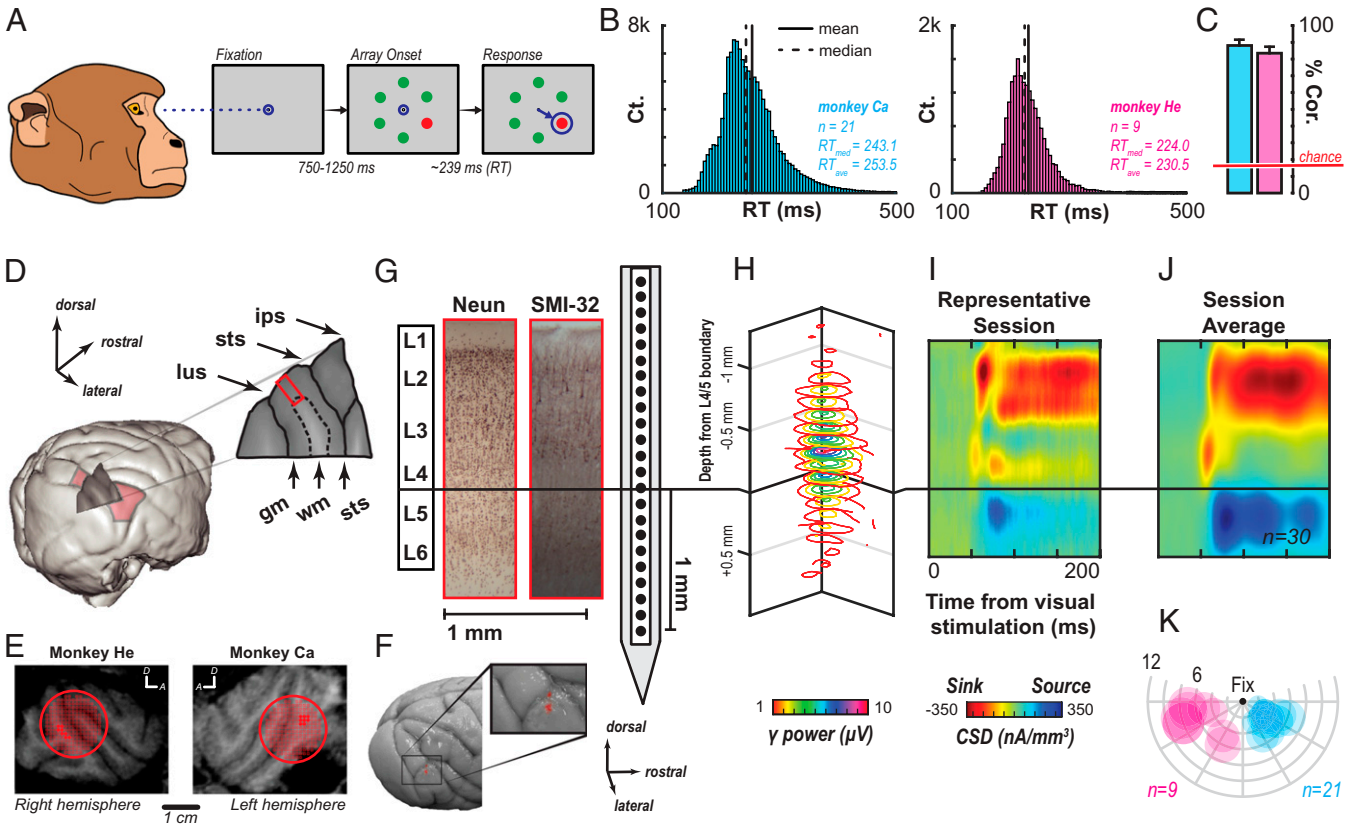

Fig. 1. (*A*) Monkeys positioned in front of a monitor fixated a central fixation dot. Following a variable delay, an array was presented. Monkeys were tasked to saccade to the oddball item to receive a juice reward. (*B*) RT distributions across all sessions for both monkeys (*Left*, cyan: monkey Ca; *Right*, magenta: He). (*C*) Behavioral performance for both monkeys across all sessions (cyan: monkey Ca; magenta: He). (*D*) (*Left*) Occipital view of a three-dimensional render of a macaque brain. Area V4 is highlighted in red. The cortical structure is revealed by the section through the prelunate gyrus. (*Right*) This slice is magnified, with additional labels indicating structural landmarks (lus, lunate sulcus; sts, superior temporal sulcus; ips, intraparietal sulcus; gm, gray matter; wm, white matter). The red box indicates a portion of V4 where linear electrode arrays can be introduced orthogonally to record across the layers of a cortical column. (*E*) MR scans for monkey He (*Left*) and monkey Ca (*Right*). The section was taken orthogonal to the 19-mm-diameter recording chamber (red outline) oriented 55° off vertical axis, 23 mm from the midline. The superior temporal sulcus can be seen running through the center of each chamber. A grid of possible penetration locations is overlaid with solid red dots indicating locations sampled in this study on the prelunate gyrus, ventroposterior to the superior temporal sulcus. (*F*) Ex vivo image of the posterior half of the brain of monkey He with expanded view of the area between lus and sts. Red marks are diiodine deposited by the final two recordings in monkey He. (*G*) Histological stains, depicting the laminar structure of V4. Labels are indicated at *Left*. Neun stain (*Left Center*) highlights the distribution of neuronal cell bodies. SMI-32 (*Right Center*) highlights pyramidal cells. (*Right*) Cartoon probe indicating the laminar positioning for neurophysiology. (*H*) RFs across recording sites of a single array penetration, indicating perpendicular penetration. (*I*) CSD profile for the same session as *H*. Current sinks are indicated in red, and sources are indicated in blue. The initial sink following visual stimulation was used as a functional marker to determine the L4/L5 boundary. The black horizontal line indicates the depth of the granular input sink. Data are smoothed along depth and across time for visualization purposes. (*J*) Mean CSD profile following alignment of the 30 sessions (21, monkey Ca; 9, He). Formatting is identical to *I*. (*K*) RF locations across sessions and monkeys (cyan, monkey Ca; magenta, He). RF centers are determined online, and diameters are estimated from previous reports. Concentric circles indicate eccentricities in degrees of visual angle. Radial lines indicate angular positions relative to central fixation.

by an accurate eye movement to, an oddball stimulus to receive a juice reward (Fig. 1*A*). Both monkeys performed the task well above chance (accuracy: monkey Ca, 88%; He, 81%) with RT consistent with previous reports of monkeys performing this task (Fig. 1 *B* and *C*; median RT: monkey Ca, 243 ms; He, 224 ms) [see previous reports for comparable behavioral data from a different cohort of macaques (57, 58)].

Laminar Recordings in V4. To evaluate the laminar profile of feature selectivity in primate area V4, we recorded neural activity throughout the layers of cortex in two macaque monkeys, using a linear electrode array with 100-μm spacing between recording contacts (Plexon S-Probe). Prior to any surgical procedures, monkeys underwent a magnetic resonance (MR) scan to identify the location of V4 (Fig. 1*D*). Following implantation of a recording chamber, monkeys underwent a second MR scan with a gadolinium-filled recording grid to identify chamber locations where an electrode could be introduced orthogonally into the prelunate gyrus (Fig. 1*E*). On each recording, we positioned and oriented the linear electrode array to span all V4 layers (Fig. 1*G*). At the end of the experiment, penetration locations were verified anatomically (Fig. 1*F*).

Monkeys performed a fixation task during which we flashed randomized, monochromatic stimuli uniform in brightness to perform reverse correlation-based RF mapping (59–61). Overlapping RFs through vertically (radially) aligned recording sites were used to confirm the perpendicular orientation of the probe (Fig. 1*H*) (59, 62). The distribution of RFs across cortex was consistent with the previously established representation of visual space on the prelunate gyrus (Fig. 1*K*) (63). To compare columns across sessions, we aligned individual recording sites relative to the granular input sink of the current source density (CSD) following visual stimulation, which identifies the boundary between the granular (L4) and infragranular (L5/6) layers of cortex (Fig. 1*I*) (61, 62, 64, 65). Ten electrode contacts including and above the L4/5 boundary and five sites below were included

for analysis. Relative to the population-based (grand average) evoked CSD profile (Fig. 1*J*), the topmost five sites corresponded to the supragranular sink, the middle five corresponded to the granular sink, and the deepest five corresponded to the infragranular source.

V4 Feature Columns. As a first step, we identified feature columns in V4. Columnar organization for color tuning has previously been reported for V4 (47, 48, 51–53). During performance of the visual search task, small, isoluminant red or green stimuli were presented within the population RF of the column (66). We estimated neural activity by evaluating high gamma power (70 Hz to 150 Hz) at each recording site, as it reliably reflects feature selectivity in visual cortex (67), arises from local circuit interactions (68), and can be reliably measured at laminar V4 recording sites, unlike single-unit or multiunit activity. To eliminate volume-conducted signals, we recalculated the locally generated gamma power from the columnar CSD (69, 70). Initially, and for the results reported in this section, these analyses were restricted to the "unattended" condition. This condition was defined as the presence of a distractor stimulus within the RF of the cortical column regardless of the position of the target in the array (five out of six array configurations where the target is outside of the RF) and when the trial was performed correctly.

To quantify the selectivity of each recording site for stimulus color, we computed the ratio of the red vs. green responses with values bounded between -1 (100% green preference) and 1 (100% red preference). Hereafter, we will refer to this as the feature selectivity index (FSI). We then calculated the mean FSI along cortical depth to compute a columnar FSI (CFSI). The CFSI quantifies the degree of feature preference across the entire column. Qualitatively, we found a high degree of consistency of columnar feature selectivity, with some columns strongly preferring red or green and other columns not distinguishing red from green (*SI Appendix*, Fig. S1*A*). To quantify this observation, we performed Wilcoxon signed-rank tests on the magnitudes of FSI along depth, where columns were deemed feature selective if $P < 0.05$. We found significant feature selectivity in 19 of 30 columns (63.3%) across both monkeys (monkey Ca, 12 of 21; He, 7 of 9).

Note that the CFSI alone does not indicate how consistent feature selectivity is within a column. To evaluate the columnar consistency of feature selectivity, we performed Bartlett's tests for the FSI variance of each column relative to the null distributions derived from 15 random samples of all measured FSIs, bootstrapped 1,000 times. The median value was taken to determine significance with $P < 0.05$. Feature selectivity was more consistent across columns than would be predicted by the null distribution in 23 of 30 columns (76.7%) across both monkeys (monkey Ca, 17 of 21; He, 6 of 9). Only 4 of 30 columns exhibited no or inconsistent selectivity across depth through these measures. We further quantified the degree of similarity within a column relative to the variance across columns by computing intraclass correlation coefficients (ICC) (71, 72). ICC reveals how consistent individual columns are in feature selectivity relative to the overall sample of V4 columns. Values toward one indicate a high degree of consistency within a column, and values toward zero indicate little to no consistency. Across the sample, we found consistency within columns to be significantly greater than chance ($\rho = 0.773, F(29, 406) = 52.19, P << 0.001$) in both monkeys (monkey Ca, $\rho = 0.848, F(20, 280) = 84.96, P << 0.001$; He, $\rho = 0.550, F(8, 112) = 19.27, P << 0.001$) (*SI Appendix*, Fig. S1*B*). For comparison, we generated shuffle control distributions of FSI values and computed the ICC. This control yielded the expected lack of consistency ($\rho = 0.003, F(999, 13986) = 1.08, P = 0.37$). These results suggest that most V4 columns are homogeneous in their feature selectivity. Lastly, we assessed the distribution of SDs of FSI across columns relative to that of the null distributions (*SI Appendix*, Fig. S1*C*). We performed a Wilcoxon signed rank test on these distributions. The result showed a significant difference ($Z = -4.02, P = 5.79e^{-5}$), providing further evidence for the homogeneity of columnar feature selectivity in V4.

We compared the feature selectivity of recorded multiunits ($n = 285$) along cortical columns to the columnar feature selectivity of each multiunit's corresponding column. We found no significant differences between the multiunit feature selectivity and multiunits' corresponding columns (Wilcoxon signed rank, $Z = 1.21, P = 0.22$) (*SI Appendix*, Fig. S2), bolstering confidence that the locally generated gamma is a useful measure of columnar feature selectivity.

To further bolster our confidence in the columnar organization for feature selectivity, we turned to Bayesian modeling. Using a Bayesian framework, we directly evaluated and compared the likelihood of several models of the organization of feature representation. Each column contributed 15 × 2 data points—one per recording site for each attention condition (which will be elaborated on in a later section). Model comparisons were based on samples of the posterior distribution from each model. The results are summarized in *SI Appendix*, Table S1. Briefly, we find that the models utilizing columnar information are more accurate in predicting the observed feature selectivity. We quantified relative model performance using the so-called leave-one-out cross-validation expected log predictive density difference (LOO-ELPD DIFF). This measure was computed between increasingly more complex models (i.e., the intercept-only model to the model incorporating all independent variables). The models without a column parameter had the lowest values and therefore performed worse than models including a column parameter. It should be noted that depth alone does not improve accuracy, as seen in the LOO-ELPD DIFF between models, indicating a lack of trends in feature selectivity within individual layers across columns. In other words, there was no observed tendency for any given layer to have a bias. These model comparisons confirm the results found through our other frequentist methods.

Laminar Variation in Strength of Feature Selectivity and Its Modulation with Attention. We next investigated whether changes in feature selectivity were observable with directed attention. To do so, we plotted the FSI for each recording site for both the unattended and attended conditions (Fig. 2*A*). The unattended condition inclusion criteria remained the same, and the attended condition was restricted to trials where the search target stimulus was present in the column's RF and the trial was performed correctly. We noticed several qualitative changes between the unattended and attended conditions (Fig. 2*A*). Many columns showed enhanced feature selectivity with attention ($n = 14$, 47%). We performed Wilcoxon signed-rank tests on the difference between the FSI between conditions across recording sites within each column ($P < 0.05$). This analysis confirmed that attending the stimulus in the RF mostly leads to enhancement of feature selectivity (Fig. 2*B*). This enhancement was so pronounced that some nonselective columns became significantly selective ($n = 6$; 20%) when attention was deployed. However, some columns did not appear to change in selectivity ($n = 13$, 43%). Fewer showed suppressed selectivity ($n = 2$, 6%) or loss of selectivity ($n = 1$, 3%). Given their small sample size, we disregard these outliers from further consideration and focus on the population of columns that were enhanced with attention.

Next, we sought to investigate laminar differences for feature selectivity and whether the enhancement associated with attention follows a distinct laminar profile. We combined recording sites within their respective laminar compartments and measured feature selectivity. Specifically, we subtracted the nCFSI from the nFSI (normalized CFSI and FSI, respectively) at each recording

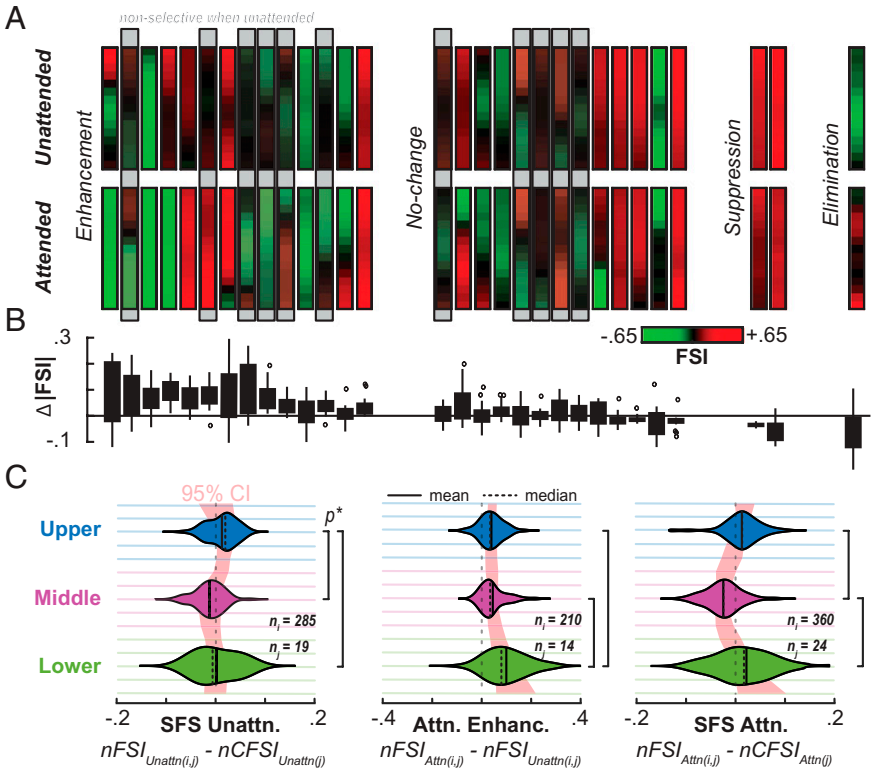

Fig. 2. (*A*) Comparing selectivity differences between unattended (*Top*) and attended (*Bottom*) conditions for each column. Each vertical color plot represents a V4 column, with the intensity of red or green denoting the strength in feature selectivity for that color. Columns are grouped by the change associated with attention: enhancement, no change, suppression, and elimination of feature selectivity, from left to right. Columns highlighted with the gray bars were columns originally measured to have no significant feature selectivity. (*B*) Box and whisker plot for the change in FSI for each recording site in each column corresponding to *A* directly above. (*C*) Laminar profiles of strength of feature selectivity (SFS). Strength of feature selectivity is taken as the difference in feature selectivity relative to the column mean, with higher values indicating stronger feature selectivity relative to the column and negative values indicating weaker feature selectivity than the column average. Recording sites were divided into their corresponding laminar compartment. Normalized feature selectivity for each of laminar compartment is shown as a violin plot for the unattended condition (*Left*, $n = 19$), the attended condition (*Right*, $n = 24$), and the enhancement from unattended to attended (*Center*, $n = 14$). Normalization was performed such that values ranged for each recording site from -1 to 1 for nonpreferred to preferred feature such that red- and green-preferring columns could be analyzed together. Solid vertical line and dashed vertical line in each distribution denote the mean and median, respectively. Red cloud behind distributions shows 95% CI cloud for strength or change in strength along depth (rather than the agglomerated compartments). Brackets to the right of each plot denote significant differences between the distributions measured by Wilcoxon signed-rank test ($P < 0.05$).

site to compute the deviation of individual V4 laminar compartments from the columnar mean (Fig. 2*C*). We performed pairwise Wilcoxon signed-rank tests of the magnitude of FSIs between the laminar compartments. We found differences between layers (upper and middle: $Z = 4.55$, $P = 5.2e^{-6}$; upper and lower: $Z = 5.19$, $P = 2.1e^{-7}$; middle and lower: $Z = 0.94$, $P = 0.34$), with upper layers exhibiting stronger feature selectivity than middle and lower layers. We used the same method to investigate the laminar profile in the attention condition (Fig. 2*C*). In the attended condition, both extragranular compartments were significantly more feature selective than the middle layers (upper and middle: $Z = 2.67$, $P = 0.007$; upper and lower: $Z = -0.96$, $P = 0.34$; middle and lower: $Z = -3.70$, $P = 2.1e^{-4}$). Accordingly, we observed the largest attentional modulation of feature selectivity in the lower layers, with the smallest in the middle and upper layers (upper and middle: $Z = -0.93$, $P = 0.35$; upper and lower: $Z = -3.80$, $P = 1.4e^{-4}$; middle and lower: $Z = -2.92$, $P = 0.0035$). Nonetheless, attentional enhancement of feature selectivity was significant in all laminar compartments as measured through Wilcoxon signed-rank tests on the differences between conditions for columns with feature selectivity (upper: $Z = 2.24$, $P = 0.02$; middle: $Z = 2.15$, $P = 0.03$; lower: $Z = 4.06$, $P = 4.9e^{-5}$).

As we do not have a reliable physiological indicator of the boundary between the middle and upper layers (like we do for middle and lower layers), one possibility might be that the 0.4 mm to 0.5 mm used for middle layer specification is not representative of the granular layer, specifically. V4's granular layer has been estimated to be thinner (73), and effects limited to the granular layer might be masked accordingly. To control for this possibility, we measured the feature selectivity, and the impacts of attention, on increasingly conservative estimates (five sites down to one). This showed that the results described above are consistent between middle-layer sizes (*SI Appendix*, Fig. S3), and granular layer-specific effects are unlikely to be masked.

Lastly, we considered Bayesian modeling again (*SI Appendix*, Table S1). Notably, addition of the attention condition, and the associated interactions, improves model performance, as the complete model, including the ATTENTION parameter, has the highest LOO-ELPD. In *SI Appendix*, Table S1, this is seen in the LOO-ELPD difference where all other models relative to the ATTENTION-sensitive model are negative (i.e., lower values). However, there are factors other than maximal model performance to consider in evaluating likelihood—model parsimony. To address model parsimony, the SE of the LOO-ELPD difference between the complete model (COLUMN × DEPTH × ATTENTION) and all other models exceeds five—indicating all terms in the model are useful. Exceeding 5 times the SE is a conservative threshold for evaluating the difference between models through this method (74).

Rhythmic Modulation of Feature Selectivity with Attention. We next sought to determine whether there was temporal variability in feature selectivity. To do so, we computed the FSI as a function of time from the peak of the transient visual response, taken as the peak of the population response averaged across recording sites and columns, to 250 ms following the stimulus array onset. We limited this analysis to the sessions found to show significant enhancement of feature selectivity with attention. We clipped the calculation at the peak of the visual transient response, as the lack of activity prior to the response results in highly variable FSI (presumably because the measure is based on a ratio). We further divvied the data into the individual laminar compartments. We noticed that there appears to be rhythmicity of selectivity along all layers—but only in the attention condition. Note that this is an oscillation in feature selectivity, not just neural activity which, if significant, would suggest feature preferences oscillate in time. Qualitatively, a beta-range (15 Hz to 30 Hz) rhythm seems to only appear in the attention condition (Fig. 3*A*). This corresponds well to a beta oscillation apparent within the locally generated high gamma signal. Quantitatively, a Fourier transform (FFT) of the temporal profile of feature selectivity in the beta range showed a significant boost in the attended condition relative to the unattended condition (Fig. 3*B*). This was observed in a subset of the data including the transient response as well as a subset excluding the transient, suggesting that this boost is not solely an artifact of the transient peak. In comparing differences between the attention conditions and layers across the beta range, we find that the beta boost linked to attention is present along all layers, albeit stronger in the middle and lower layers than the upper layers (Wilcoxon signed rank, $P < 0.05$). All differences are depicted in Fig. 3*C*. Interestingly, the beta rhythm survives a difference computation (Fig. 3*D*)—meaning the same rhythmicity is not present, or at least mostly attenuated, in the unattended condition. Performing a Fourier fit on the temporal profiles of enhancement in feature selectivity at a beta frequency suggests the enhancement contains a beta oscillatory component, as these model fits better explain the enhancement than a model without a time-varying component (R^2: Fourier fit, upper = 0.33, middle = 0.45, lower = 0.38; intercept-only fit, upper = $-1.1e^{-13}$, middle = $4.9e^{-13}$, lower = $-5.3e^{-15}$). Importantly, the rhythmic modulation of feature selectivity did not depend on microsaccades (*SI Appendix*, Fig. S4), suggesting this is not simply a result of motor-related activity.

Laminar Origins for the Synaptic Currents Generating the Beta Rhythm. As a next step, we sought to determine whether there are changes in synaptic activity that might relate to the generation of the beta oscillation. To do so, we identified troughs in the nonrecalculated beta oscillation (to avoid circular analysis) on a trial-by-trial level and extracted the time-locked CSD, as an estimate of synaptic activation, for both the attended and unattended conditions (Fig. 4). We found a significant current sink in middle and upper layers, time locked to beta troughs in both conditions. Specifically, we computed *t* tests over time, where significance was defined as 10 consecutive milliseconds of $P < 0.05$. Electrode contacts within each laminar compartment were averaged for computing statistics. In computing the difference between the resultant spatiotemporal profiles of CSD, we found that the superficial current sink was significantly stronger in the attention condition using the same criteria. Moreover, this significant difference largely preceded the beta trough, perhaps indicative of a causal relationship. Thus, beta-driven activation seems to be linked to synaptic interactions in the upper layers of V4.

Beta Coupling. We sought to better characterize the rhythmic activity during this task. We first plotted the gamma power

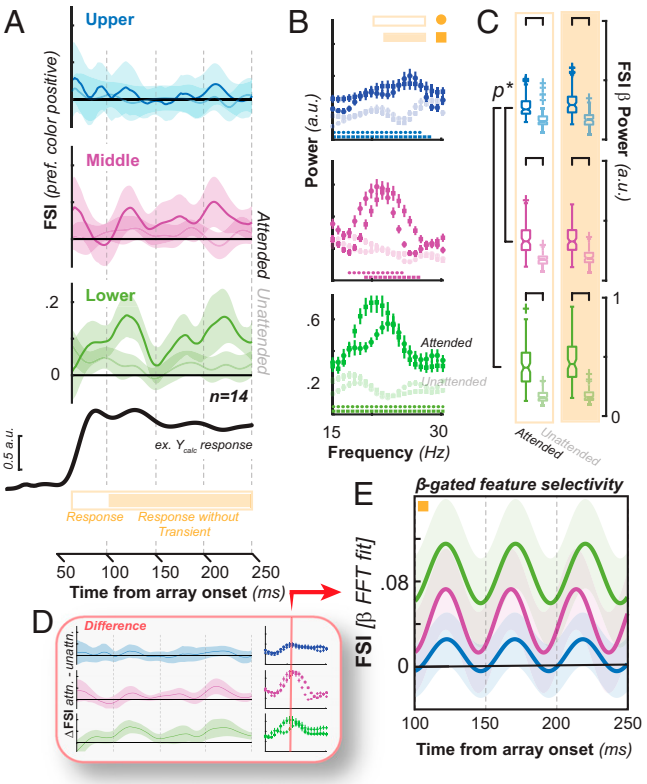

Fig. 3. (*A*) Temporal profile of high gamma feature selectivity across sessions found to have significant enhancement of feature selectivity with attention (left, $n = 14$). Traces are shown from time since stimulus array onset. Upper-, middle-, and lower-layer compartments are shown in blue, magenta, and green, respectively. Attended condition is shown as opaque lines, and unattended condition is shown as translucent. The 95% CIs are shown as clouds around the lines. Black trace shows example locally generated high gamma power response for reference relative in time to the FSI traces. Orange bar at the bottom indicates RT periods including transient (60 ms to 250 ms) and excluding transient (100 ms to 250 ms) for subsequent analysis. (*B*) Normalized power from FFT of the temporal profiles of FSI in the beta frequency band for the attended (opaque) and unattended (translucent) conditions. Circles denote FFT on data including transient, and square denotes data excluding transient. Dotted lines at bottom of each plot denote significant difference between attended and unattended conditions for the respective datasets ($P < 0.05$). (*C*) Summary differences between conditions and layers for the beta FSI power (15 Hz to 30 Hz) taken as the average for respective conditions in *B*. Data in orange outline are including transient, and data in orange fill are excluding transient. Brackets denote $P < 0.05$ in Wilcoxon signed-rank test indicating differences between attention conditions and differences between relative power in beta-oscillating feature selectivity between layers. (*D*) Difference in temporal profiles of feature selectivity between attention conditions and corresponding FFT in beta range indicating oscillation exists in attention condition and not unattended. (*E*) Fourier fit of temporal profile of feature selectivity for the response excluding transient at the frequency with peak power across the laminar compartments taken from the difference measures in *D*. Clouds denote 90% prediction intervals of the model fits.

responses along depth, averaged across sessions for both the attended and unattended conditions (Fig. 5*B*). We next confirmed that these gamma responses were significantly modulated by attention, by performing a *t* test across time, where significance was defined as $P < 0.05$ for 10 consecutive milliseconds. We noticed a beta-range rhythm along all layers in both conditions. To confirm this observation, we filtered the gamma power in the beta frequency band (15 Hz to 30 Hz) and plotted the result (Fig. 5*B*). This transformation yields beta modulation of gamma power, hereafter referred to as gamma–beta. We noticed that

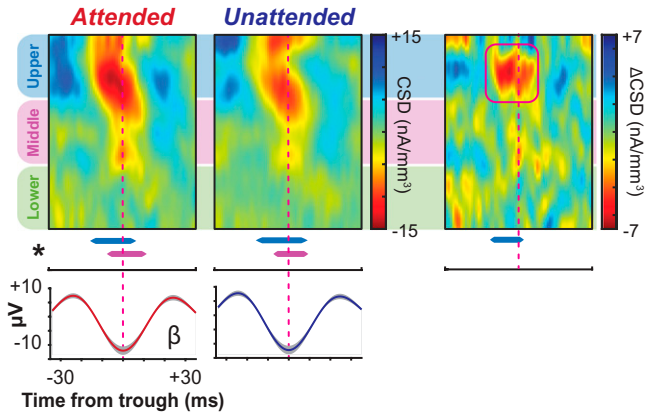

Fig. 4. (*Left* and *Center*) Synaptic activation measured as CSD for the attended and unattended conditions locked to beta for each respective condition averaged across sessions ($n = 30$). Beta rhythm shown here is taken as the average across recording channels along the cortical column with 95% CI. Current sink is observable in the upper and middle layers of cortex coupled to beta. (*Right*) Difference between attended and unattended conditions. Greater activation in the upper layers is observable in the attention condition highlighted with an outline. Significant synaptic activation and difference between conditions is shown below each color plot. Blue line represents upper-layer CSD, and magenta line represents middle-layer CSD. Abscissa are uniform throughout each plot.

there was no significant difference between the gamma–beta in the attended and unattended conditions (conditions detailed in Fig. 5*A*). Hence, although beta rhythmicity of feature selectivity is exclusive to the attention condition, beta modulation of the gamma response occurred with or without attention.

We then measured coupling between gamma power along V4 layers and beta. These analyses were limited to low-frequency oscillations during the sustained response (100 ms to 250 ms following array onset), to eliminate confounds related the transient response. First, we observed beta power along layers for both attention conditions (Fig. 5*C*). We then performed a Wilcoxon signed-rank test between each of the possible combinations of pairs of laminar compartments to determine whether there was a significant difference in beta ($P < 0.05$). We found that beta power was stronger in the extragranular compartments than the granular and strongest in the lower layers, coinciding with the strongest beta modulation of feature selectivity. At the same time, we determined whether there was a significant difference in beta power along the layers between conditions (Wilcoxon signed rank; $P < 0.05$). This analysis revealed a significant difference between attention conditions across all layers. We then computed the coupling between gamma and beta within the upper layers of cortex—where the beta-generating CSD was found (Fig. 5*D*). We found that gamma power along all layers was coupled to the upper-layer beta oscillation to a significant degree. However, there was no observable difference in the spatiotemporal profiles between attention conditions. In other words, attention does not seem to modulate beta frequency coupling of V4 neuronal responses, which eliminates a simple, response timing-related explanation for attentional gating of feature selectivity. To ensure this finding was beta specific, we also measured the spatiotemporal profile of power in other low-frequency bands—specifically, alpha (8 Hz to 15 Hz) and high theta (7 Hz to 8 Hz)—as well as their coupling with the gamma activity (*SI Appendix*, Fig. S5). We found the profiles of power were not identical across frequency bands, nor were the coupling profiles similar. This suggests that our findings are specific to the beta band and not due to generalized broadband low-frequency coupling.

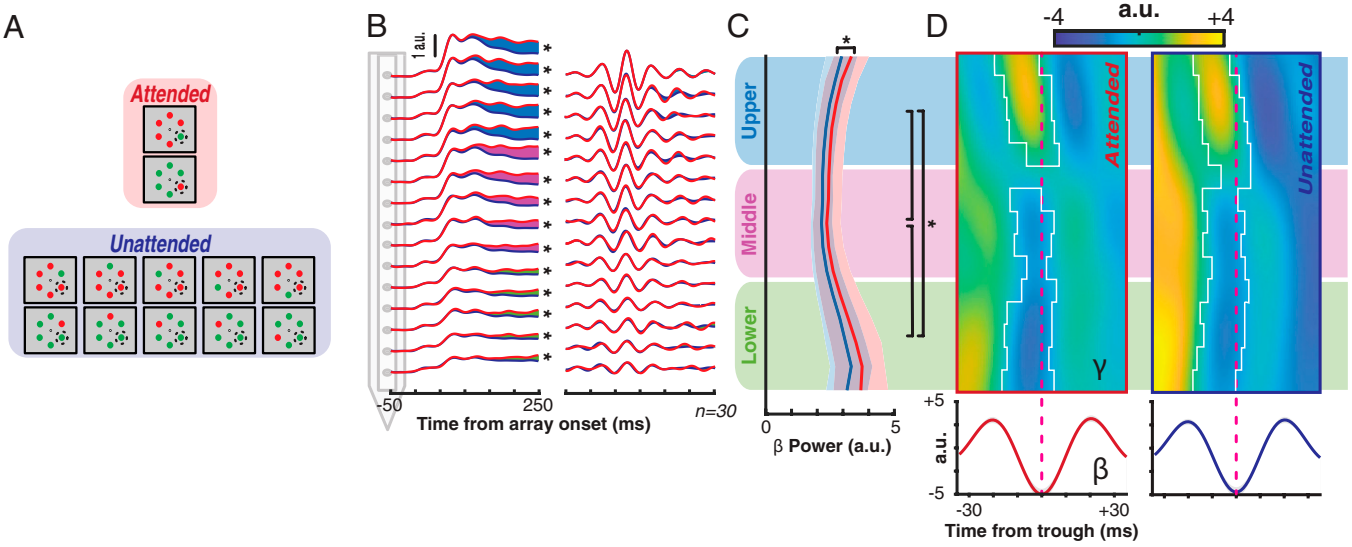

Fig. 5. (*A*) Search array configurations and their respective attention condition assignment. (*B*) (*Left*) Temporal profile of gamma power shown across recording sites averaged across cortical columns ($n = 30$) from time since stimulus array onset. Upper, middle, and lower compartments are shown as the top five, middle five, and bottom five traces, respectively. Attended condition is shown as red lines, and unattended condition is shown in blue. Significant difference between attended and unattended conditions observed across all recording sites are denoted by an asterisk next to each pair of traces measured through *t* test through time, where $P < 0.05$ for more than 10 ms. Gamma power responses filtered in the beta band (15 Hz to 30 Hz) shown at right, referred to hereafter as gamma-beta. (*Right*) Beta rhythm observable across both conditions along all recording sites with no measurable significant differences between traces through the same method. (*C*) Strength of beta power (not gamma–beta) along recording sites for attended (red) and unattended (blue) conditions taken as the average 100 ms to 250 ms following array onset. Significant difference is denoted at right between attended and unattended conditions through a Wilcoxon signed-rank test ($P < 0.05$). Brackets show significant differences in beta power strength between laminar compartments regardless of attention condition. (*D*) Gamma power across recording sites (*Top*) coupled to the upper layers beta oscillation (*Bottom*) (mean and 95% CI cloud) for the attended (*Left*) and unattended (*Right*) conditions taken as the average across sessions ($n = 30$). Significant coupling is shown as outline through *t* test along recording sites and samples relative to beta trough, with a Bonferroni correction applied. Significant coupling between gamma power and beta oscillation is observed in both attention conditions around the time of the beta trough along all layers.

Gamma–Beta Strength Predicts Behavior. Low-frequency oscillations have been linked to performance during attention tasks (34, 75–82). We thus investigated whether low frequencies, specifically those measurable in the locally generated gamma response, were linked to the animals' behavioral output. Given the coupling between gamma and beta (Fig. 5), we suspected beta as the most promising candidate for a relationship with behavior. To see whether this was the case, we extended our investigation to other low frequencies (theta and alpha). For this analysis, we used the power estimates from the FFT of high gamma as predictors, and used RT (i.e., initiation time of saccade to target) to measure behavioral outcome. Only correct trials were considered, and trials in the unattended condition were subsampled to match the attended condition. To evaluate these potential relationships, we turned to a form of multiple linear regression.

We used a proportional odds logistic regression (POLR) model to assess the relationship between low-frequency power in the gamma response and behavioral outcome. This structure allowed us to vincentize the RT data, and corresponding neural data, into quartiles (i.e., the fastest 25%, the faster 25%, the slower 25%, and the slowest 25% of trials), and treat it as an ordered factor outcome. In this structure, each recording site contributed four data points (one for each vincentized bin) for each evaluated condition. Results of this approach are summarized in Table 1. The model was fit with the three (theta, alpha, beta) low-frequency power measures as independent variables, each interacted with attention condition and tested under frequentist and Bayesian frameworks. A negative coefficient indicates that stronger magnitude of that frequency modulating the locally generated gamma response is associated with faster RT, and vice versa. We found that both beta power and alpha power were significantly predictive of RT in the attended condition. As beta power increased, RT decreased. As alpha power increased, RT increased. In the unattended case, none of the low-frequency powers were associated with RT. As we have found laminar dependencies in previous analyses, we also tested models including depth as an interaction term with each of the low-frequency oscillatory independent variables; however, they did not improve model performance (likelihood ratio tests of ordinal regression models: $LR(20) = 22.82, P = 0.30$), which is why we report the more parsimonious model here. Of most import to this study, these findings demonstrate the beta rhythm modulating the neural response is associated with behavior, but only with attention—paralleling our finding regarding the beta-gated feature selectivity.

Discussion

Sensory responses in visual cortical microcircuits are modified with attention (5–12, 14–17, 19–22, 62, 83). We sought to understand how feature selectivity is modified in an attention task. To do so, we focused on the columnar microcircuit of V4. We found that enhancement of feature selectivity occurred across the layers of cortex, albeit with variable magnitude. Interestingly, this enhancement was coupled to several cycles of a beta oscillation in the local field potential. Notably, the coupling of feature selectivity to beta oscillations in the neural response was not present in the unattended condition. In other words, feature selectivity only oscillated in synchrony with the beta rhythm when attention was deployed, reminiscent of prior reports where attention-related behavior was linked to low-frequency oscillations in neural activity (13, 75, 77, 79, 84–92). Our findings demonstrate mechanistically that low-frequency rhythms in attentional performance are linked not just to response magnitude but also to periodic changes in feature selectivity (tuning) in visual cortex.

As an initial step in our study, we identified columnar cortical representations for feature selectivity in area V4. Previous work testing for the existence of color columns yielded conflicting results (44, 47–50); however, the more recent studies ubiquitously support their existence (51–53). Our findings confirm these recent conclusions. It is perhaps worth noting the value in our approach to this question. That is, none of the previous studies recorded neurons simultaneously along the layers of V4, as orthogonal penetrations of V4 are notoriously difficult. Thus, virtually all prior findings relied on indirect assessments of columnar functional architecture. Using MR-guided linear array recordings, we were able to measure simultaneous activity along V4 columns and thus confirm the existence of color columns. Moreover, our results shed some light on discrepancies in previous results. Specifically, we found that different columns prefer different colors, and that they do so at different relative strengths. This finding reconciles both previous functional imaging studies (93–95) and prior neurophysiological studies on color selectivity in V4 (47–49, 96–99). The variability we found at the laminar level might explain the conflicting results regarding the magnitude of selectivity across studies using differing methodological approaches. That is, we found that, despite the existence of color columns, the strength of selectivity for a specific color along depth is not uniform. Instead, V4's upper layers generally show stronger selectivity than the lower layers—but only in the unattended condition. This is consistent with previous findings along a different feature dimension—namely, orientation tuning (100)—perhaps suggesting a common attribute of feature processing in the absence of attention. Taken together, our results demonstrate that, despite the existence of color columns, V4 color selectivity varies considerably in both the tangential and the radial dimension.

Table 1. Strength of oscillatory activity modulating locally generated high gamma predicts behavioral responses when attended

		Frequentist			Bayesian	
Model term	Value [SE]	*t*	*P*	95% CI	Median	95% Credible Interval
$\gamma - \theta$ (theta, 7 Hz to 8 Hz, a.u.): unattend	−81.8 [97.1]	−0.84	0.40	−272.1, 108.4	−82.9	−599.9, 431.3
$\gamma - \alpha$ (alpha, 8 Hz to 15 Hz, a.u.): unattend	−8.8 [77.6]	−0.11	0.91	−160.9, 143.9	−64.2	−642.2, 520.6
$\gamma - \beta$ (beta, 15 Hz to 30 Hz, a.u.): unattend	40.5 [59.3]	0.68	0.49	−75.7, 156.7	70.9	−323.1, 467.5
$\gamma - \theta$ (theta, 7 Hz to 8 Hz, a.u.): attend	−29.9 [92.5]	−0.31	0.75	−210.3, 152.4	78.6	−548.9, 702.1
$\gamma - \alpha$ (alpha, 8 Hz to 15 Hz, a.u.): attend	326.9 [73.1]	4.47	**$7.7e^{-4}$**	183.7, 470.3	284.6	−357.1, 930.8
$\gamma - \beta$ (beta, 15 Hz to 30 Hz, a.u.): attend	−342.9 [40.49]	−8.47	**$2.4e^{-17}$**	−422.3, −263.6	−330.1	**−605.4, −65.1**

Results of multiple linear regression in the form of POLR. Both the frequentist and Bayesian forms of the POLR were tested. Model was designed to fit vincentized RT using three coefficients: power in theta (θ), alpha (α), and beta (β) derived from an FFT of the locally generated gamma power (γ). These were interacted with attention condition. Data from both monkeys ($n = 2$) across all sessions ($n = 30$) were included. Each recording site ($n = 450$) contributed 24 data points (4 vincentized bins × 3 modulating frequencies × 2 attention conditions). Significant coefficients are displayed in red (frequentist form, *P* column; Bayesian form, 95% Credible Interval column), with direction of relationship between coefficient and outcome indicated as negative or positive numbers in the value column.

One important limitation of the current study when considering precision in these color representations is that we were limited to testing only two colors out of the entire gamut available to trichromats. Moreover, our determination of isoluminance was based on a human ideal observer rather than psychophysical testing of each animal. Many of our conclusions thus are based on the assumptions 1) that there were little to no luminance differences between our stimuli that could explain our results in the absence of hue selectivity and 2) that the evidence for red and green color columns can be extended to other parts of the color spectrum as well. We believe that assumption 1 can be justified by the fact that the absorption spectra of macaque and human L and M cones differ negligibly (101) (but see ref. 102) and that direct psychophysical evaluation suggests that humans and macaques perceive colors similarly (103). Importantly, evidence that we gathered from indirect measures suggested that luminance varied negligibly. Both RT (104) and neural response latencies (105) vary with luminance of stimuli. In our dataset, we find no variability in these measures between the red and green stimuli (*SI Appendix*, Table S2). Furthermore, previous work has found no support for a functional organization for luminance in V4 (51), making our interpretation, that the columnar organization we observe is due to color selectivity rather than luminance, the more parsimonious conclusion. Nonetheless, it is important to note that it cannot entirely be ruled out that at least some of the results we obtained are due to differences in luminance rather than hue. Similarly, while assumption 2 remains largely a conjecture, it rests on our direct findings for colors red and green as well as the array of previous studies providing indirect evidence for V4 color columns across a wider area of the gamut (47, 48, 52, 53). Further investigation is necessary to determine whether the laminar differences we found extend to different colors. Furthermore, given the representation and tuning for color varies across the cortical sheet (106) and the limited portion of V4 where orthogonal laminar recordings can easily be achieved, additional variability might exist beyond what we observed here. While more general questions regarding the nuances of the laminar organization of color selectivity remain, the finding that V4 columns act as functional microcircuits for the processing of different color stimuli is consistent with the principles of a canonical cortical microcircuit (54–56).

Perhaps our most surprising result was not just that the attention-enhanced feature selectivity fluctuated in a beta rhythm but also that the beta rhythm was present in our neural activity regardless of attention condition. This result might suggest that the beta rhythm observed in our data is not necessarily generated through a cognitive process but is rather more associated with sensory or perceptual processing. Support for this conclusion can be found in other work. Notably, direct modification of low-frequency neural oscillations in V4 through optogenetics impairs perception (107). However, other work suggests that these low-frequency oscillations are top-down in origin and regulate the enhancement of bottom-up responses (108) and are not dependent on early visual cortical areas (109). Other studies more generally suggest a top-down role for beta activity with respect to attention (110–114), subjective visual detection (115, 116), working memory (117, 118), and other phenomena involving feedback (119). As our data are limited to V4, we cannot directly test for a source for the beta oscillations. It is noteworthy, however, that the beta rhythm in both attention conditions has associated current sinks in both the granular, feedforward input layer and the superficial layers of cortex. Perhaps more insight can be gained from exploring the putative functional architecture that would be supporting these findings, as well as the instantiating mechanism.

One consideration is the array of afferent and efferent connections of V4. Area V4 seemingly assumes an important position in the visual cortical hierarchy with respect to attentional selection and modulation when considering its anatomical connections. It shows attentional modulation across various tasks and has connections to both earlier and later visual cortical areas, as well as connections to frontal attentional control structures (97, 120–122). Moreover, these frontal structures have a demonstrable impact on sensory processing in V4 (123). For example, inactivation of frontal eye field (FEF) at sites corresponding retinotopically to recorded V4 neurons reveals that FEF contributes to the presaccadic specification of visual target features (124). Also of note is that inactivation of ventral prearcuate areas (VPA) in frontal cortex eliminates effects of feature attention in V4 (125).

Assuming the beta oscillation we describe has a prefrontal origin, the target of frontal feedback connections to V4 would likely be the extragranular layers (54–56, 126), which coincides with where we observe the difference in beta-generating CSD. However, it is worth noting that the deep layers of V4 have previously been shown to be most associated with behavioral outcome (100), whereas the behavior-associated synaptic activity in our study was located to the upper layers of V4. This apparent discrepancy could be reconciled by upper-layer synaptic activity perhaps driving apical dendrites from deep-layer visual cortical neurons (127). Regardless, the extragranular nature of this signal might suggest that top-down connections play a role in our findings.

Models of visual attentional selection promote an important role for area V4 interacting with other visual cortical and frontal areas (128). With these connections and interactions in mind, the connections between frontal areas like FEF or VPA and V4 are one likely source for the mechanism manifesting the frequency gating we observe in sensory processing and seem a good candidate for further investigation. Specifically, frontal attentional control structures might excite V4 in a beta-rhythmic fashion and with laminar specificity such that targets of attention are enhanced only with that rhythm. That is, frontal structures could regulate the bottom-up neural response such that the recipients of V4 output are more sensitive to behaviorally relevant information. However, recent work also provides causal evidence of a role of posterior parietal cortex in pop-out modulation and the saccadic selection of salient stimuli (129). Given the interconnectivity of V4 and parietal areas (121) coupled with these findings, posterior parietal cortex becomes another possible source for the results reported here.

Recent reports have demonstrated a link between spiking activity and low-frequency oscillations that is predictive of behavioral outcome in frontoparietal attention networks (130). Given the similarity with our findings, it seems a link could be hypothesized between this network and the sensory processing stage we document here. However, it is important to note that their findings were restricted to visuomovement neurons in FEF. In another attention task, visual neurons in FEF, but not movement or visuomovement neurons, showed enhanced gamma-frequency synchronization with activity in V4 (89). Yet, it may also be that the populations of functional cell types in FEF are more nuanced than previously thought, so alternative labeling of these populations might reveal a link through functional mappings (131). While speculative, this hypothesis can be tested empirically to determine whether there is a direct link between the behavior-associated beta found in the oculomotor system and that found at the sensory processing stage documented here.

In considering possible instantiating mechanism neural pathways, it is also useful to consider the nature and conditions of the attention allocation. Specifically, do these findings arise from an endogenous, goal-directed process or from an exogenous, stimulus-driven mechanism? Pop-out singleton stimuli are known to capture attention (132, 133). The exogenous factors of the task used in this study are known to modulate V4 activity when endogenous factors are controlled for (134), but endogenous saccadic preparation can also modulate V4 activity (135).

Thus, the findings of this paper could result through exogenous or endogenous means.

Speculatively, an exogenous mechanism seems most plausible. This rests on three independent observations: 1) The animals' task was efficient pop-out search, which is thought to involve exogenous, stimulus-driven attention (136). 2) The V4 response to the array of visual stimuli comprises a beta component regardless of attention condition, suggesting that attention-related feedback is not necessary for beta-range rhythmicity to emerge in V4. 3) The beta-modulated feature selectivity arises within the initial transient response, before feedback can evolve. To bolster support for observation 3, enhancement of feature selectivity should be present before feedback activity [about 100 ms following array onset (137, 138); see *SI Appendix*, Fig. S6]. Sensory cortex may be sufficient to select the attentional target in this task without frontal or parietal help. Models of exogenous selection can locate salient items solely through local lateral inhibition (e.g., refs. 139 and 140). Taken together, these factors are consistent with the conjecture that the beta-gated enhancement with attention arises through a bottom-up process. It is noteworthy that slow, rhythmic fluctuations of V4 responses coupled to attention have previously been shown to emerge through competitive interactions between neighboring neurons (82). However, as noted, the dissociation of exogenous and endogenous attentional components in this task is indirect, so further work is required to disentangle them.

Materials and Methods

All procedures were in accordance with the NIH Guidelines and the Association for Assessment and Accreditation of Laboratory Animal Care International's *Guide for the Care and Use of Laboratory Animals* (141) and approved by the Vanderbilt Institutional Animal Care and Use Committee in accordance with US Department of Agriculture and US Public Health Service policies. Two adult male macaque monkeys (*Macaca radiata*; monkey Ca, 7.5 kg; He, 7.3 kg) performed pop-out visual searches while neural data were collected from area V4 on the prelunate gyrus using linear multielectrode arrays. Complete documentation of the materials and methods used to perform this study can be found in *SI Appendix*. *SI Appendix* includes sections on the following: Surgical Procedures and MRI, V4 Localization, Stimuli and Task, Neurophysiological Procedure, Receptive Field Mapping, CSD and Laminar Alignment, Locally Generated Gamma Recalculation, Feature Selectivity Index, Feature Selectivity Index Statistics, Intraclass Correlation Coefficient, Layer Comparisons, Bayesian Modeling, Fourier Transform of Feature Selectivity Index and High Gamma Response, Microsaccade Detection, Proportional Odds Logistic Regression Modeling, Cross-frequency Coupling and Beta-locked CSD, Multiunit Activity, and Materials Availability.

Data Availability. Neurophysiology data have been deposited in Dryad (DOI: 10.5061/dryad.3r2280gh4).

ACKNOWLEDGMENTS. This work was supported by the National Eye Institute (Awards R01EY027402, R01EY019882, R01EY008890, and P30EY008126). J.A.W. was supported by fellowships from the National Eye Institute (Fellowships F31EY031293 and T32EY007135). We would like to thank M.F., I.H., M.M., S.M., D.R., M.S., L.T., B.W., and R.W. for technical support. We would also like to thank B.C., L.D., S.E., K.L., B.M., T.R., A.S., G.W., and P.M. for useful conversations regarding the work.

1. D. H. Hubel, T. N. Wiesel, Receptive fields, binocular interaction and functional architecture in the cat's visual cortex. *J. Physiol.* **160**, 106–154 (1962).
2. D. H. Hubel, T. N. Wiesel, Receptive fields and functional architecture of monkey striate cortex. *J. Physiol.* **195**, 215–243 (1968).
3. D. H. Hubel, T. N. Wiesel, S. LeVay, Plasticity of ocular dominance columns in monkey striate cortex. *Philos. Trans. R. Soc. Lond. B Biol. Sci.* **278**, 377–409 (1977).
4. J. H. Kaas, Plasticity of sensory and motor maps in adult mammals. *Annu. Rev. Neurosci.* **14**, 137–167 (1991).
5. R. Desimone, J. Duncan, Neural mechanisms of selective visual attention. *Annu. Rev. Neurosci.* **18**, 193–222 (1995).
6. C. J. McAdams, J. H. Maunsell, Effects of attention on orientation-tuning functions of single neurons in macaque cortical area V4. *J. Neurosci.* **19**, 431–441 (1999).
7. C. J. McAdams, J. H. Maunsell, Attention to both space and feature modulates neuronal responses in macaque area V4. *J. Neurophysiol.* **83**, 1751–1755 (2000).
8. S. Treue, J. C. Martínez Trujillo, Feature-based attention influences motion processing gain in macaque visual cortex. *Nature* **399**, 575–579 (1999).
9. S. Kastner, L. G. Ungerleider, Mechanisms of visual attention in the human cortex. *Annu. Rev. Neurosci.* **23**, 315–341 (2000).
10. G. H. Recanzone, R. H. Wurtz, Effects of attention on MT and MST neuronal activity during pursuit initiation. *J. Neurophysiol.* **83**, 777–790 (2000).
11. J. H. Reynolds, L. Chelazzi, R. Desimone, Competitive mechanisms subserve attention in macaque areas V2 and V4. *J. Neurosci.* **19**, 1736–1753 (1999).
12. J. H. Reynolds, T. Pasternak, R. Desimone, Attention increases sensitivity of V4 neurons. *Neuron* **26**, 703–714 (2000).
13. P. Fries, J. H. Reynolds, A. E. Rorie, R. Desimone, Modulation of oscillatory neuronal synchronization by selective visual attention. *Science* **291**, 1560–1563 (2001).
14. J. Martínez-Trujillo, S. Treue, Attentional modulation strength in cortical area MT depends on stimulus contrast. *Neuron* **35**, 365–370 (2002).
15. J. H. Reynolds, R. Desimone, Interacting roles of attention and visual salience in V4. *Neuron* **37**, 853–863 (2003).
16. J. H. Reynolds, L. Chelazzi, Attentional modulation of visual processing. *Annu. Rev. Neurosci.* **27**, 611–647 (2004).
17. T. Williford, J. H. Maunsell, Effects of spatial attention on contrast response functions in macaque area V4. *J. Neurophysiol.* **96**, 40–54 (2006).
18. J. Y. Cohen, R. P. Heitz, J. D. Schall, G. F. Woodman, On the origin of event-related potentials indexing covert attentional selection during visual search. *J. Neurophysiol.* **102**, 2375–2386 (2009).
19. J. H. Reynolds, D. J. Heeger, The normalization model of attention. *Neuron* **61**, 168–185 (2009).
20. A. M. Ni, J. H. R. Maunsell, Spatially tuned normalization explains attention modulation variance within neurons. *J. Neurophysiol.* **118**, 1903–1913 (2017).
21. A. M. Ni, J. H. R. Maunsell, Neuronal effects of spatial and feature attention differ due to normalization. *J. Neurosci.* **39**, 5493–5505 (2019).
22. I. Sani, E. Santandrea, M. C. Morrone, L. Chelazzi, Temporally evolving gain mechanisms of attention in macaque area V4. *J. Neurophysiol.* **118**, 964–985 (2017).
23. P. R. Roelfsema, V. A. Lamme, H. Spekreijse, Object-based attention in the primary visual cortex of the macaque monkey. *Nature* **395**, 376–381 (1998).
24. D. Wegener, W. A. Freiwald, A. K. Kreiter, The influence of sustained selective attention on stimulus selectivity in macaque visual area MT. *J. Neurosci.* **24**, 6106–6114 (2004).
25. P. R. Roelfsema, M. Tolboom, P. S. Khayat, Different processing phases for features, figures, and selective attention in the primary visual cortex. *Neuron* **56**, 785–792 (2007).
26. P. Fries, T. Womelsdorf, R. Oostenveld, R. Desimone, The effects of visual stimulation and selective visual attention on rhythmic neuronal synchronization in macaque area V4. *J. Neurosci.* **28**, 4823–4835 (2008).
27. D. Rotermund, K. Taylor, U. A. Ernst, A. K. Kreiter, K. R. Pawelzik, Attention improves object representation in visual cortical field potentials. *J. Neurosci.* **29**, 10120–10130 (2009).
28. A. Thiele, A. Pooresmaeili, L. S. Delicato, J. L. Herrero, P. R. Roelfsema, Additive effects of attention and stimulus contrast in primary visual cortex. *Cereb. Cortex* **19**, 2970–2981 (2009).
29. A. Pooresmaeili, J. Poort, A. Thiele, P. R. Roelfsema, Separable codes for attention and luminance contrast in the primary visual cortex. *J. Neurosci.* **30**, 12701–12711 (2010).
30. M. R. Cohen, J. H. Maunsell, Using neuronal populations to study the mechanisms underlying spatial and feature attention. *Neuron* **70**, 1192–1204 (2011).
31. J. Poort *et al.*, The role of attention in figure-ground segregation in areas V1 and V4 of the visual cortex. *Neuron* **75**, 143–156 (2012).
32. L. Stănişor, C. van der Togt, C. M. Pennartz, P. R. Roelfsema, A unified selection signal for attention and reward in primary visual cortex. *Proc. Natl. Acad. Sci. U.S.A.* **110**, 9136–9141 (2013).
33. M. Vinck, T. Womelsdorf, E. A. Buffalo, R. Desimone, P. Fries, Attentional modulation of cell-class-specific gamma-band synchronization in awake monkey area v4. *Neuron* **80**, 1077–1089 (2013).
34. D. Ferro, J. van Kempen, M. Boyd, S. Panzeri, A. Thiele, Directed information exchange between cortical layers in macaque V1 and V4 and its modulation by selective attention. *Proc. Natl. Acad. Sci. U.S.A.* **118**, e2022097118 (2021).
35. D. H. Hubel, T. N. Wiesel, Sequence regularity and geometry of orientation columns in the monkey striate cortex. *J. Comp. Neurol.* **158**, 267–293 (1974).
36. W. Vanduffel, R. B. Tootell, A. A. Schoups, G. A. Orban, The organization of orientation selectivity throughout macaque visual cortex. *Cereb. Cortex* **12**, 647–662 (2002).
37. S. LeVay, D. H. Hubel, T. N. Wiesel, The pattern of ocular dominance columns in macaque visual cortex revealed by a reduced silver stain. *J. Comp. Neurol.* **159**, 559–576 (1975).
38. R. B. Tootell, S. L. Hamilton, Functional anatomy of the second visual area (V2) in the macaque. *J. Neurosci.* **9**, 2620–2644 (1989).
39. R. B. H. Tootell, S. Nasr, Columnar segregation of magnocellular and parvocellular streams in human extrastriate cortex. *J. Neurosci.* **37**, 8014–8032 (2017).
40. D. L. Adams, S. Zeki, Functional organization of macaque V3 for stereoscopic depth. *J. Neurophysiol.* **86**, 2195–2203 (2001).
41. T. D. Albright, R. Desimone, C. G. Gross, Columnar organization of directionally selective cells in visual area MT of the macaque. *J. Neurophysiol.* **51**, 16–31 (1984).
42. G. C. DeAngelis, W. T. Newsome, Organization of disparity-selective neurons in macaque area MT. *J. Neurosci.* **19**, 1398–1415 (1999).
43. J. Liu, W. T. Newsome, Functional organization of speed tuned neurons in visual area MT. *J. Neurophysiol.* **89**, 246–256 (2003).
44. M. Tanaka, H. Weber, O. D. Creutzfeldt, Visual properties and spatial distribution of neurones in the visual association area on the prelunate gyrus of the awake monkey. *Exp. Brain Res.* **65**, 11–37 (1986).
45. I. Fujita, K. Tanaka, M. Ito, K. Cheng, Columns for visual features of objects in monkey inferotemporal cortex. *Nature* **360**, 343–346 (1992).

46. K. Tanaka, Columns for complex visual object features in the inferotemporal cortex: Clustering of cells with similar but slightly different stimulus selectivities. *Cereb. Cortex* **13**, 90–99 (2003).
47. S. M. Zeki, Colour coding in rhesus monkey prestriate cortex. *Brain Res.* **53**, 422–427 (1973).
48. S. Zeki, The representation of colours in the cerebral cortex. *Nature* **284**, 412–418 (1980).
49. S. J. Schein, R. T. Marrocco, F. M. de Monasterio, Is there a high concentration of color-selective cells in area V4 of monkey visual cortex? *J. Neurophysiol.* **47**, 193–213 (1982).
50. T. Yoshioka, B. M. Dow, Color, orientation and cytochrome oxidase reactivity in areas V1, V2 and V4 of macaque monkey visual cortex. *Behav. Brain Res.* **76**, 71–88 (1996).
51. R. B. Tootell, K. Nelissen, W. Vanduffel, G. A. Orban, Search for color 'center(s)' in macaque visual cortex. *Cereb. Cortex* **14**, 353–363 (2004).
52. B. R. Conway, D. Y. Tsao, Color-tuned neurons are spatially clustered according to color preference within alert macaque posterior inferior temporal cortex. *Proc. Natl. Acad. Sci. U.S.A.* **106**, 18034–18039 (2009).
53. Y. Kotake, H. Morimoto, Y. Okazaki, I. Fujita, H. Tamura, Organization of color-selective neurons in macaque visual area V4. *J. Neurophysiol.* **102**, 15–27 (2009).
54. R. J. Douglas, K. A. C. Martin, D. Whitteridge, A canonical microcircuit for neocortex. *Neural Comput.* **1**, 480–488 (1989).
55. R. J. Douglas, K. A. C. Martin, A functional microcircuit for cat visual cortex. *J. Physiol.* **440**, 735–769 (1991).
56. A. M. Bastos *et al.*, Canonical microcircuits for predictive coding. *Neuron* **76**, 695–711 (2012).
57. B. A. Purcell, P. K. Weigand, J. D. Schall, Supplementary eye field during visual search: Salience, cognitive control, and performance monitoring. *J. Neurosci.* **32**, 10273–10285 (2012).
58. J. A. Westerberg, A. Maier, G. F. Woodman, J. D. Schall, Performance monitoring during visual priming. *J. Cogn. Neurosci.* **32**, 515–526 (2020).
59. M. A. Cox *et al.*, Spiking suppression precedes cued attentional enhancement of neural responses in primary visual cortex. *Cereb. Cortex* **29**, 77–90 (2019).
60. K. Dougherty, M. A. Cox, J. A. Westerberg, A. Maier, Binocular modulation of monocular v1 neurons. *Curr. Biol.* **29**, 381–391.e4 (2019).
61. J. A. Westerberg, M. A. Cox, K. Dougherty, A. Maier, V1 microcircuit dynamics: Altered signal propagation suggests intracortical origins for adaptation in response to visual repetition. *J. Neurophysiol.* **121**, 1938–1952 (2019).
62. A. S. Nandy, J. J. Nassi, J. H. Reynolds, Laminar organization of attentional modulation in macaque visual area v4. *Neuron* **93**, 235–246 (2017).
63. R. Gattass, A. P. B. Sousa, C. G. Gross, Visuotopic organization and extent of V3 and V4 of the macaque. *J. Neurosci.* **8**, 1831–1845 (1988).
64. C. E. Schroeder, A. D. Mehta, S. J. Givre, A spatiotemporal profile of visual system activation revealed by current source density analysis in the awake macaque. *Cereb. Cortex* **8**, 575–592 (1998).
65. A. Maier, G. K. Adams, C. Aura, D. A. Leopold, Distinct superficial and deep laminar domains of activity in the visual cortex during rest and stimulation. *Front. Syst. Neurosci.* **4**, 31 (2010).
66. J. A. Westerberg, A. Maier, J. D. Schall, Priming of attentional selection in macaque visual cortex: Feature-based facilitation and location-based inhibition of return. *eNeuro* **7**, ENUURO.0466-19.2020 (2020).
67. P. Berens, G. A. Keliris, A. S. Ecker, N. K. Logothetis, A. S. Tolias, Feature selectivity of the gamma-band of the local field potential in primate primary visual cortex. *Front. Neurosci.* **2**, 199–207 (2008).
68. S. Ray, J. H. Maunsell, Differences in gamma frequencies across visual cortex restrict their possible use in computation. *Neuron* **67**, 885–896 (2010).
69. C. Nicholson, R. Llinas, Field potentials in the alligator cerebellum and theory of their relationship to Purkinje cell dendritic spikes. *J. Neurophysiol.* **34**, 509–531 (1971).
70. Y. Kajikawa, C. E. Schroeder, How local is the local field potential? *Neuron* **72**, 847–858 (2011).
71. P. E. Shrout, J. L. Fleiss, Intraclass correlations: Uses in assessing rater reliability. *Psychol. Bull.* **86**, 420–428 (1979).
72. K. O. McGraw, S. P. Wong, Forming inferences about some intraclass correlation coefficients. *Psychol. Methods* **1**, 30–46 (1996).
73. P. R. Hof, J. H. Morrison, Neurofilament protein defines regional patterns of cortical organization in the macaque monkey visual system: A quantitative immunohistochemical analysis. *J. Comp. Neurol.* **352**, 161–186 (1995).
74. Y. Bengio, Y. Grandvalet, "No unbiased estimator of the variance of K-fold cross-validation" in *Advances in Neural Information Processing Systems*, S. Thrun, K. Saul, B. Scholkopf, Eds. (MIT Press, Cambridge, MA, 2004) vol. 16, pp. 513–520.
75. A. N. Landau, P. Fries, Attention samples stimuli rhythmically. *Curr. Biol.* **22**, 1000–1004 (2012).
76. Y. B. Saalmann, M. A. Pinsk, L. Wang, X. Li, S. Kastner, The pulvinar regulates information transmission between cortical areas based on attention demands. *Science* **337**, 753–756 (2012).
77. I. C. Fiebelkorn, Y. B. Saalmann, S. Kastner, Rhythmic sampling within and between objects despite sustained attention at a cued location. *Curr. Biol.* **23**, 2553–2558 (2013).
78. I. C. Fiebelkorn, M. A. Pinsk, S. Kastner, A dynamic interplay within the frontoparietal network underlies rhythmic spatial attention. *Neuron* **99**, 842 (2018).
79. I. C. Fiebelkorn, S. Kastner, A rhythmic theory of attention. *Trends Cogn. Sci.* **23**, 87–101 (2019).
80. I. C. Fiebelkorn, M. A. Pinsk, S. Kastner, The mediodorsal pulvinar coordinates the macaque fronto-parietal network during rhythmic spatial attention. *Nat. Commun.* **10**, 215 (2019).
81. R. F. Helfrich *et al.*, Neural mechanisms of sustained attention are rhythmic. *Neuron* **99**, 854–865.e5 (2018).
82. R. Kienitz *et al.*, Theta rhythmic neuronal activity and reaction times arising from cortical receptive field interactions during distributed attention. *Curr. Biol.* **28**, 2377–2387.e5 (2018).
83. J. C. Martinez-Trujillo, S. Treue, Feature-based attention increases the selectivity of population responses in primate visual cortex. *Curr. Biol.* **14**, 744–751 (2004).
84. T. Womelsdorf, P. Fries, The role of neuronal synchronization in selective attention. *Curr. Opin. Neurobiol.* **17**, 154–160 (2007).
85. P. Lakatos, G. Karmos, A. D. Mehta, I. Ulbert, C. E. Schroeder, Entrainment of neuronal oscillations as a mechanism of attentional selection. *Science* **320**, 110–113 (2008).
86. J. J. Foxe, A. C. Snyder, The role of alpha-band brain oscillations as a sensory suppression mechanism during selective attention. *Front. Psychol.* **2**, 154 (2011).
87. C. E. Schroeder, D. A. Wilson, T. Radman, H. Scharfman, P. Lakatos, Dynamics of active sensing and perceptual selection. *Curr. Opin. Neurobiol.* **20**, 172–176 (2010).
88. R. Vanrullen, J. Dubois, The psychophysics of brain rhythms. *Front. Psychol.* **2**, 203 (2011).
89. G. G. Gregoriou, S. J. Gotts, R. Desimone, Cell-type-specific synchronization of neural activity in FEF with V4 during attention. *Neuron* **73**, 581–594 (2012).
90. M. S. Clayton, N. Yeung, R. Cohen Kadosh, The roles of cortical oscillations in sustained attention. *Trends Cogn. Sci.* **19**, 188–195 (2015).
91. P. Fries, Rhythms for cognition: Communication through coherence. *Neuron* **88**, 220–235 (2015).
92. A. Zalta, S. Petkoski, B. Morillon, Natural rhythms of periodic temporal attention. *Nat. Commun.* **11**, 1051 (2020).
93. B. R. Conway, S. Moeller, D. Y. Tsao, Specialized color modules in macaque extrastriate cortex. *Neuron* **56**, 560–573 (2007).
94. A. Wade, M. Augath, N. Logothetis, B. Wandell, fMRI measurements of color in macaque and human. *J. Vis.* **8**, 1–19 (2008).
95. H. Tanigawa, H. D. Lu, A. W. Roe, Functional organization for color and orientation in macaque V4. *Nat. Neurosci.* **13**, 1542–1548 (2010).
96. S. J. Schein, R. Desimone, Spectral properties of V4 neurons in the macaque. *J. Neurosci.* **10**, 3369–3389 (1990).
97. A. W. Roe *et al.*, Toward a unified theory of visual area V4. *Neuron* **74**, 12–29 (2012).
98. S. Liebe, N. K. Logothetis, G. Rainer, Dissociable effects of natural image structure and color on LFP and spiking activity in the lateral prefrontal cortex and extrastriate visual area V4. *J. Neurosci.* **31**, 10215–10227 (2011).
99. B. N. Bushnell, A. Pasupathy, Shape encoding consistency across colors in primate V4. *J. Neurophysiol.* **108**, 1299–1308 (2012).
100. W. W. Pettine, N. A. Steinmetz, T. Moore, Laminar segregation of sensory coding and behavioral readout in macaque V4. *Proc. Natl. Acad. Sci. U.S.A.* **116**, 14749–14754 (2019).
101. B. J. Nunn, J. L. Schnapf, D. A. Baylor, Spectral sensitivity of single cones in the retina of *Macaca fascicularis*. *Nature* **309**, 264–266 (1984).
102. K. R. Dobkins, A. Thiele, T. D. Albright, Comparison of red-green equiluminance points in humans and macaques: Evidence for different L:M cone ratios between species. *J. Opt. Soc. Am. A Opt. Image Sci. Vis.* **17**, 545–556 (2000).
103. G. Gagin *et al.*, Color-detection thresholds in rhesus macaque monkeys and humans. *J. Vis.* **14**, 12 (2014).
104. T. Tanaka, S. Nishida, T. Aso, T. Ogawa, Visual response of neurons in the lateral intraparietal area and saccadic reaction time during a visual detection task. *Eur. J. Neurosci.* **37**, 942–956 (2013).
105. W. S. Geisler, D. G. Albrecht, A. M. Crane, Responses of neurons in primary visual cortex to transient changes in local contrast and luminance. *J. Neurosci.* **27**, 5063–5067 (2007).
106. K. S. Bohon, K. L. Hermann, T. Hansen, B. R. Conway, Representation of perceptual color space in macaque posterior inferior temporal cortex (the V_4 complex). *eNeuro* **3**, 28 (2016).
107. A. Nandy, J. J. Nassi, M. P. Jadi, J. Reynolds, Optogenetically induced low-frequency correlations impair perception. *eLife* **8**, e35123 (2019).
108. C. G. Richter, W. H. Thompson, C. A. Bosman, P. Fries, Top-down beta enhances bottom-up gamma. *J. Neurosci.* **37**, 6698–6711 (2017).
109. J. T. Schmiedt *et al.*, Beta oscillation dynamics in extrastriate cortex after removal of primary visual cortex. *J. Neurosci.* **34**, 11857–11864 (2014).
110. F. H. Lopes da Silva, A. van Rotterdam, W. Storm van Leeuwen, A. M. Tielen, Dynamic characteristics of visual evoked potentials in the dog. II. Beta frequency selectivity in evoked potentials and background activity. *Electroencephalogr. Clin. Neurophysiol.* **29**, 260–268 (1970).
111. M. Bekisz, A. Wróbel, Attention-dependent coupling between beta activities recorded in the cat's thalamic and cortical representations of the central visual field. *Eur. J. Neurosci.* **17**, 421–426 (2003).
112. T. J. Buschman, E. K. Miller, Top-down versus bottom-up control of attention in the prefrontal and posterior parietal cortices. *Science* **315**, 1860–1862 (2007).
113. C. A. Bosman *et al.*, Attentional stimulus selection through selective synchronization between monkey visual areas. *Neuron* **75**, 875–888 (2012).
114. I. Grothe, S. D. Neitzel, S. Mandon, A. K. Kreiter, Switching neuronal inputs by differential modulations of gamma-band phase-coherence. *J. Neurosci.* **32**, 16172–16180 (2012).
115. M. Wilke, N. K. Logothetis, D. A. Leopold, Local field potential reflects perceptual suppression in monkey visual cortex. *Proc. Natl. Acad. Sci. U.S.A.* **103**, 17507–17512 (2006).
116. A. Maier *et al.*, Divergence of fMRI and neural signals in V1 during perceptual suppression in the awake monkey. *Nat. Neurosci.* **11**, 1193–1200 (2008).
117. C. Tallon-Baudry, S. Mandon, W. A. Freiwald, A. K. Kreiter, Oscillatory synchrony in the monkey temporal lobe correlates with performance in a visual short-term memory task. *Cereb. Cortex* **14**, 713–720 (2004).

118. R. F. Salazar, N. M. Dotson, S. L. Bressler, C. M. Gray, Content-specific fronto-parietal synchronization during visual working memory. *Science* **338**, 1097–1100 (2012).
119. A. K. Engel, P. Fries, Beta-band oscillations—Signalling the status quo? *Curr. Opin. Neurobiol.* **20**, 156–165 (2010).
120. J. D. Schall, A. Morel, D. J. King, J. Bullier, Topography of visual cortex connections with frontal eye field in macaque: Convergence and segregation of processing streams. *J. Neurosci.* **15**, 4464–4487 (1995).
121. L. G. Ungerleider, T. W. Galkin, R. Desimone, R. Gattass, Cortical connections of area V4 in the macaque. *Cereb. Cortex* **18**, 477–499 (2008).
122. P. Pouget *et al.*, Visual and motor connectivity and the distribution of calcium-binding proteins in macaque frontal eye field: Implications for saccade target selection. *Front. Neuroanat.* **3**, 2 (2009).
123. T. Moore, K. M. Armstrong, Selective gating of visual signals by microstimulation of frontal cortex. *Nature* **421**, 370–373 (2003).
124. B. Noudoost, K. L. Clark, T. Moore, A distinct contribution of the frontal eye field to the visual representation of saccadic targets. *J. Neurosci.* **34**, 3687–3698 (2014).
125. N. P. Bichot, R. Xu, A. Ghadooshahy, M. L. Williams, R. Desimone, The role of prefrontal cortex in the control of feature attention in area V4. *Nat. Commun.* **10**, 5727 (2019).
126. J. C. Anderson, H. Kennedy, K. A. C. Martin, Pathways of attention: Synaptic relationships of frontal eye field to V4, lateral intraparietal cortex, and area 46 in macaque monkey. *J. Neurosci.* **31**, 10872–10881 (2011).
127. V. B. Mountcastle, The columnar organization of the neocortex. *Brain* **120**, 701–722 (1997).
128. F. H. Hamker, The reentry hypothesis: The putative interaction of the frontal eye field, ventrolateral prefrontal cortex, and areas V4, IT for attention and eye movement. *Cereb. Cortex* **15**, 431–447 (2005).
129. X. Chen *et al.*, Parietal cortex regulates visual salience and salience-driven behavior. *Neuron* **106**, 177–187.e4 (2020).
130. I. C. Fiebelkorn, S. Kastner, Spike timing in the attention network predicts behavioral outcome prior to target selection. *Neuron* **109**, 177–188.e4 (2021).
131. K. A. Lowe, J. D. Schall, Functional categories of visuomotor neurons in macaque frontal eye field. *eNeuro* **5**, ENEURO.0131–18.2018 (2018).
132. J. Theeuwes, Cross-dimensional perceptual selectivity. *Percept. Psychophys.* **50**, 184–193 (1991).
133. J. D. Cosman, K. A. Lowe, W. Zinke, G. F. Woodman, J. D. Schall, Prefrontal control of visual distraction. *Curr. Biol.* **28**, 414–420.e3 (2018).
134. B. E. Burrows, T. Moore, Influence and limitations of popout in the selection of salient visual stimuli by area V4 neurons. *J. Neurosci.* **29**, 15169–15177 (2009).
135. N. A. Steinmetz, T. Moore, Eye movement preparation modulates neuronal responses in area V4 when dissociated from attentional demands. *Neuron* **83**, 496–506 (2014).
136. M. M. Chun, J. M. Wolfe, "Visual attention" in *Blackwell Handbook of Sensation and Perception*, E. B. Goldstein, Ed. (Blackwell, 2001), pp. 272–310.
137. A. D. Mehta, I. Ulbert, C. E. Schroeder, Intermodal selective attention in monkeys. II: Physiological mechanisms of modulation. *Cereb. Cortex* **10**, 359–370 (2000).
138. A. D. Mehta, I. Ulbert, C. E. Schroeder, Intermodal selective attention in monkeys. I: Distribution and timing of effects across visual areas. *Cereb. Cortex* **10**, 343–358 (2000).
139. L. Itti, C. Koch, A saliency-based search mechanism for overt and covert shifts of visual attention. *Vision Res.* **40**, 1489–1506 (2000).
140. A. Soltani, C. Koch, Visual saliency computations: Mechanisms, constraints, and the effect of feedback. *J. Neurosci.* **30**, 12831–12843 (2010).
141. National Research Council, *Guide for the Care and Use of Laboratory Animals* (National Academies Press, Washington, DC, ed. 8, 2011).